

Mott transition in Modulated Lattices and Parent Insulator of $(\text{K,Tl})_y\text{Fe}_x\text{Se}_2$ Superconductors

Rong Yu,¹ Jian-Xin Zhu,² and Qimiao Si¹

¹*Department of Physics & Astronomy, Rice University, Houston, Texas 77005*

²*Theoretical Division, Los Alamos National Laboratory, Los Alamos, New Mexico 87545*

The degree of electron correlations remains a central issue in the iron-based superconductors. The parent iron pnictides are antiferromagnetic, and their bad-metal behavior has been interpreted in terms of proximity to a Mott transition. We study such a transition in multi-orbital models on modulated lattices containing an ordered pattern of iron vacancies, using a slave-rotor method. We show that the ordered vacancies lead to a band-narrowing, which pushes the system to the Mott insulator side. This effect is proposed to underlie the insulating behavior observed in the parent compounds of the newly discovered $(\text{K,Tl})_y\text{Fe}_x\text{Se}_2$ superconductors.

Introduction. Superconductivity in the layered iron pnictides and chalcogenides occurs near antiferromagnetically-ordered parent compounds [1–3]. In their paramagnetic phase, these parent materials have a large electrical resistivity corresponding to an in-plane carrier mean-free-path on the order of the inverse Fermi wavevector. They also show a strong reduction of the Drude weight [4], and temperature-induced spectral weight transfer that extends to high energies (on the eV order) [5–7]. Such bad-metal behavior is characteristic of metallic systems in proximity to a Mott transition [8–10]

Recently, superconductivity has been discovered in a new family of iron-based compounds $\text{K}_y\text{Fe}_2\text{Se}_2$ [11] and related $(\text{K,Tl})\text{Fe}_x\text{Se}_2$ [12]. In these compounds the maximal superconducting transition temperature is comparable to that of the 122 iron pnictides. Similarly to the pnictides, the superconductivity occurs close to an antiferromagnetically ordered state [12]. At the same time, these materials are unique in several aspects. Both the angle-resolved photoemission (ARPES) experiments [13–15] and LDA calculations [16] show that the Fermi surface has only electron pockets. The absence of hole Fermi pockets is unique among the iron based superconductors, raising hope for major new and general insights to be gained from studying these materials. Equally important, the Fe vacancies may form ordered patterns when the Fe content $x \lesssim 1.6$ as suggested by various experiments [12, 17, 18]. Furthermore, there are parent compounds which are insulating [12, 19]. The control parameter that tunes the $(\text{K,Tl})\text{Fe}_x\text{Se}_2$ system from superconducting to insulating is the Fe composition x , and $x = 1.5$ is the primary candidate composition for a parent compound. There is evidence [12, 17] that in $(\text{K,Tl})\text{Fe}_{1.5}\text{Se}_2$ the Fe vacancies form regular patterns possibly as illustrated in either Fig. 1(b) or Fig. 1(c). The in-plane electrical resistivity is about two orders of magnitude larger than that of the parent iron pnictides at room temperature, and it further increases exponentially as temperature is lowered. The insulating behavior is also manifested in the optical conductivity [20], which is strongly suppressed below about 0.7 eV. Because of experimental indications that the (K,Tl) content is also variable, we will in the following refer to these systems as $(\text{K,Tl})_y\text{Fe}_x\text{Se}_2$.

In this Letter, we propose that the parent $(\text{K,Tl})_y\text{Fe}_{1.5}\text{Se}_2$ is a Mott insulator arising from a correlation effect that is enhanced by the Fe vacancies. We describe the ordered Fe va-

cancies in terms of a modulated lattice, and introduce a two-orbital model with two electrons per Fe site to capture their electronic structure. We use a slave-rotor method to show that a Mott transition exists in this model even though there are an even number of electrons per site (and per unit cell). We find that the interaction strength for the Mott transition largely tracks the electronic bandwidth. In other words, ordered Fe vacancies enhance the tendency towards Mott localization as a result of a kinetic-energy reduction. Such Fe vacancies, therefore, have a similar effect as a lattice expansion, which we have previously discussed as responsible for the Mott insulating behavior in $\text{La}_2\text{O}_3\text{Fe}_2\text{Se}_2$ [21]. Our considerations of the interaction effects are realistic, given that the *ab initio* calculations using density-functional theory [22] show that the 3d bands of $\text{TlFe}_{1.5}\text{Se}_2$ are narrower than those of TlFe_2Se_2 .

Modulated lattices and kinetic-energy reduction. We will consider a square lattice (L1, Fig. 1(a)), a modulated square lattice consisting of 2×2 plaquettes each having its center removed (L2, Fig. 1(b)), and another one corresponding to a triangular lattice of such 2×2 plaquettes (L3, Fig 1(c)).

The $(\text{K,Tl})_y\text{Fe}_x\text{Se}_2$ system involves all five 3d orbitals. The ARPES experiments [13–15] show electron pockets near M point and suggest very weak electron-like pockets near Γ point. The absence of hole pocket near Γ point is largely consistent with the *ab initio* electronic bandstructure calculations using local-density-approximation (LDA) for $(\text{K,Tl})\text{Fe}_2\text{Se}_2$ [16, 23–26]. This is in contrast to the case of iron pnictides, and is easier to model using a two-orbital tight-binding parametrization. Correspondingly, we consider a two-orbital model with the degenerate xz and yz orbitals (labeled as orbitals 1 and 2) and $n = 2$. Inspired by the considerations in the pnictides case [27, 28], we introduce a set of tight-binding parameters. The parameters are listed in Table I, and their meanings can be inferred from the dispersion functions specified in Eq. (2). We first fit the LDA bandstructure obtained on TlFe_2Se_2 to this two-orbital model and then adjust the tight-binding model parameters so that the Fermi surface still has only electron pockets at $n = 2$. We notice that the Fermi surface size is larger than in the bandstructure calculations, but this suffices for our qualitative considerations of the effect of lattice depletion on the Mott transition. What is important is that, for our parameters, the Fermi surface comprises only electron pockets near the X points of the 1-Fe per cell Brill-

louni Zone. The bandwidth narrowing for L2 and L3 lattices compared to the L1 lattice is shown in Fig. 1(e).

intra-orbital (eV)				inter-orbital (eV)	
t_1	t_2	t_3	t_9	t_4	t_{12}
0.093	0.081	-0.222	-0.038	0.023	-0.038

TABLE I. Hopping parameters of the two-orbital model.

Two-orbital model and the slave-rotor method. We are now in position to specify our model,

$$\mathcal{H} = - \sum_{ij, \alpha\beta, \sigma} t_{ij}^{\alpha\beta} c_{i\alpha\sigma}^\dagger c_{j\beta\sigma} + \frac{U}{2} \sum_i \left(\sum_{\alpha\sigma} n_{\alpha\sigma} \right)^2 \quad (1)$$

where $c_{i\alpha\sigma}$ annihilates an electron in orbital α and spin σ on site i of the Fe lattice. The first term in Eq. (1) describes the electron hopping, with orbital dependent hopping amplitudes

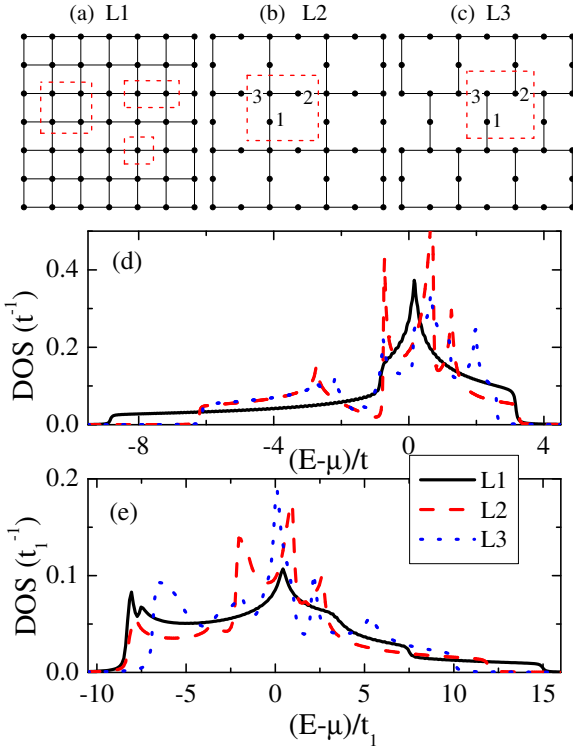


FIG. 1. (Color online) a) Square lattice, L1. Different clusters are used and will be labeled as $N_c = 1, 2,$ and $4,$ respectively; b) Modulated 2×2 square lattice, L2. The enclosed sites 1,2,3 form the basis of the unit cell; c) Another modulated 2×2 lattice, L3 (corresponding to a 4×2 superstructure in the FeSe plane). Also shown are the bare density-of-states (DOS) for the one-orbital model ($t = t' = 1$) (d) and the two-orbital model (e).

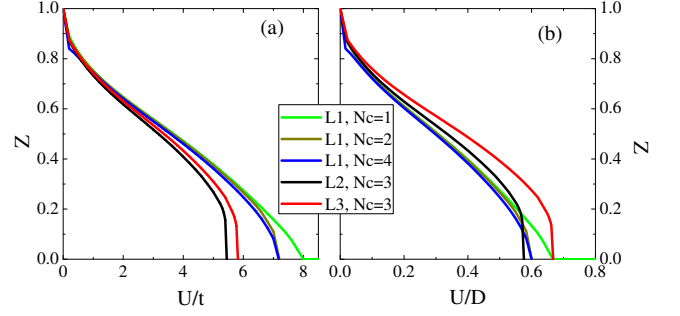


FIG. 2. (Color online) Quasiparticle weight for the one-orbital model in the unmodulated and modulated lattices plotted as a function of U/t (a) and U/D (b).

$t_{ij}^{\alpha\beta} = t_1, t_2, \dots, t_{12}$ yielding $\sum_{k\alpha\beta\sigma} \epsilon_{k\sigma}^{\alpha\beta} c_{k\alpha\sigma}^\dagger c_{k\alpha\sigma}$, where

$$\begin{aligned} \epsilon_k^{11} &= -2t_1 \cos k_x - 2t_2 \cos k_y - 4t_3 \cos k_x \cos k_y \\ &\quad - 4t_9 \cos 2k_x \cos 2k_y, \\ \epsilon_k^{22} &= -2t_2 \cos k_x - 2t_1 \cos k_y - 4t_3 \cos k_x \cos k_y \\ &\quad - 4t_9 \cos 2k_x \cos 2k_y, \\ \epsilon_k^{12} &= \epsilon_k^{21} = -4t_4 \sin k_x \sin k_y - 4t_{12} \sin 2k_x \sin 2k_y. \end{aligned} \quad (2)$$

Small hoppings t_9 and t_{12} between the 5th-nearest neighbors are included to reproduce the two electron pockets at $n = 2$. The second term in Eq. (1) is an on-site Coulomb repulsion. We focus on the effect of lattice depletion on the Mott transition and will not consider Hund's coupling and pair-hopping terms for simplicity. All local interactions are expected to have effects similar to U . In particular, the Hund's coupling will reduce the critical U of the Mott transition; its effects are readily studied within a slave-spin method [29, 30], and the results will be reported elsewhere.

We study the model using the cluster slave-rotor mean-field (CSRMF) method [31, 32]. We introduce an $O(2)$ rotor variable θ_i and a spinon $f_{i\alpha\sigma}$ on each site, and write $c_{i\alpha\sigma} = f_{i\alpha\sigma} e^{-i\theta_i}$. Here, $e^{-i\theta_i}$ lowers the rotor angular momentum L_i , which corresponds to the charge quantum number. The unphysical states are eliminated by enforcing the constraint $L_i = \sum_{\alpha\sigma} (f_{i\alpha\sigma}^\dagger f_{i\alpha\sigma} - 1/2)$ in the enlarged rotor and spinon Hilbert space. By rewriting Eq. (1) using rotor and spinon operators and decoupling the rotor and spinon operators at the mean-field level, we obtain the following two effective Hamiltonians:

$$\begin{aligned} H_f &= - \sum_{ij\alpha\beta\sigma} t_{ij}^{\alpha\beta} C_{ij} f_{i\alpha\sigma}^\dagger f_{j\beta\sigma} - (\mu + \lambda) \sum_{i\alpha\sigma} n_{i\alpha\sigma}^f, \quad (3) \\ H_\theta &= -2 \sum_{ij} t_{ij}^{\alpha\beta} \chi_{ij}^{\alpha\beta} e^{i(\theta_i - \theta_j)} + \frac{U}{2} \sum_i L_i^2 + \lambda \sum_i L_i, \quad (4) \end{aligned}$$

where $C_{ij} \equiv \langle e^{i(\theta_i - \theta_j)} \rangle_\theta$ is the rotor correlation function that renormalizes the quasiparticle hopping parameters in the presence of interaction, $\chi_{ij}^{\alpha\beta} \equiv \langle f_{i\alpha\sigma}^\dagger f_{j\beta\sigma} \rangle_f$, μ is the chemical potential, and λ is a Lagrange multiplier to impose the constraint. To solve these two Hamiltonians, which still contain

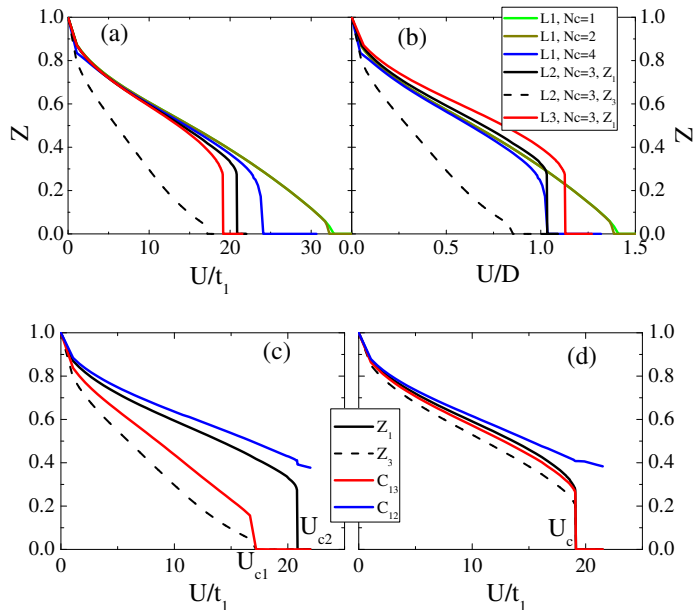


FIG. 3. (Color online) Quasiparticle weight Z for the two-orbital model vs. U/t (a) and U/D (b). Also shown are the site-selective Z_1 and Z_3 and the bond correlations for lattices L2 (c) and L3 (d).

interactions among rotors, we further apply a cluster mean-field approximation. We exactly diagonalize the rotor Hamiltonian on a finite cluster, and treat the influence of the sites outside the cluster as a mean field. We decouple $e^{i(\theta_i - \theta_j)}$ into $e^{i\theta_i} \phi_j$ if i belongs to the cluster but j is outside. Here $\phi_i \equiv \langle e^{-i\theta_i} \rangle$ is the local mean-field parameter. Consequently, C_{ij} is factorized as $C_{ij} \approx \phi_i^* \phi_j$ if either i or j is outside the cluster. In practice, Eqs. (3) and (4) are self-consistently solved by iteratively determining the mean-field parameters ϕ_i , C_{ij} , and $\chi_{ij}^{\alpha\beta}$. The Mott transition is signaled by a vanishing quasiparticle spectral weight $Z = |\phi_i|^2$.

To gain intuition on the role of the lattice modulation, we will also study a one-orbital model with nearest-neighbor hopping, t , and next-nearest-neighbor hopping, t' . Fig. 1(d) illustrates the reduction of the bandwidth for L2 and L3 lattices from that of the L1 lattice, for the case of $t' = t$. A non-zero t' is chosen for two reasons. It avoids a perfect nesting in the case of $n = 1$, which we study below. It also avoids a flat band in the case of the L2 lattice: when $t' = 0$, for the L2 lattice, there are two dispersive bands with a combined bandwidth of $4\sqrt{2}t$, and a flat band in the middle.

Results for the one-orbital model. We start from the one-orbital case. Because the L2 and L3 lattices involve a 2×2 square plaquette as the unit cell, we will carry out our calculations for the lattice L1 with $N_c = 4$. The slave-rotor mean-field theory treats the rotor kinetic energy for intra-cluster bonds exactly by diagonalizing the rotor Hamiltonian on the cluster. Hence working with $N_c = 4$ gives a better description of the Mott transition than using the single site approximation. Fig. 2(a) shows the renormalized quasiparticle weight, Z , as

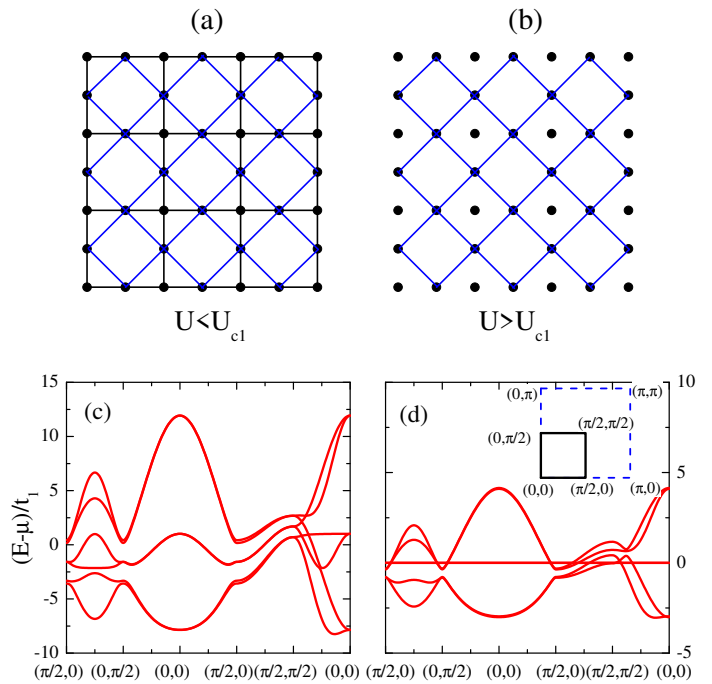


FIG. 4. (Color online) Sketch of the renormalized hoppings for the L2 lattice at $U < U_{c1}$ (a) and at $U_{c1} < U < U_{c2}$ (b). Also shown are the bandstructure of L2 for $U = 0 < U_{c1}$ (c) and for $U_{c1} < U = 19t_1 < U_{c2}$ (d). The bands are shown along the high-symmetry directions in the Brillouin Zone associated with the 2×2 -Fe unit cell, illustrated in the inset in (d).

a function of U/t . The Mott transition occurs at U_c , where Z first goes to zero as U is increased. For the L1 lattice, increasing the cluster size from $N_c = 1$ to $N_c = 4$ leads to a successive reduction of U_c : $U_c \approx 8t$ for $N_c = 1$, and $U_c \approx 7.2t$ for $N_c = 4$.

On the modulated lattices, we also find a Mott transition. It is seen that $U_c \approx 5.4t$ for the L2 lattice and $U_c \approx 5.8t$ for L3 lattice; both are smaller than that of the L1 lattice.

Fig. 2(b) plots the same result, but with U now normalized against the full bandwidth D . It is seen that U_c/D is comparable for all three cases. This clearly illustrates that the reduction of U_c for the modulated L2 and L3 lattices arises from the band-narrowing effect.

Results for the two-orbital model. We now turn to the more realistic two-orbital case. The renormalized quasiparticle weight as a function of U/t_1 is shown in Fig. 3(a). It is again seen that the values of U_c for both the L2 and L3 lattices are smaller than that of the L1 lattice with $N_c = 4$.

One difference from the toy 1-orbital model is that the hopping parameters in the two-orbital model are highly anisotropic (e.g., $|t_3/t_2| \approx 3$), which makes the local environment possibly different from site to site on the modulated lattices. To fully address the influence of the inhomogeneity, we study the quasiparticle weight associated with each site in the cluster $Z_i = |\langle e^{i\theta_i} \rangle|^2$. For either L1 or L3, we ob-

tain a single Mott transition as in the one-orbital case. For the L2 lattice, we find two transitions. They are identified by the vanishing of Z_3 first at $U_{c1}/t_1 \approx 17$, and subsequently the vanishing of Z_1 (and, equivalently, Z_2) at a higher value $U_{c2}/t_1 \approx 20$.

To understand this, we have in the same figure plotted the bond correlators C_{12} and C_{13} . Between U_{c1} and U_{c2} , C_{13} vanishes but C_{12} remains finite. This makes site 3 to be unconnected to the rest of the lattice (*cf.* Fig. 4(b)). We see these explicitly in a plot of the renormalized bandstructure in Fig. 4(d): associated with the isolated 3 sites is a flat band lying exactly on the Fermi level for $U_{c1} < U < U_{c2}$. By contrast, for $U < U_{c1}$, all sites are connected by hopping terms (Fig. 4(a)) and there exists no flat band (Fig. 4(c)).

For the L3 lattice, the geometry prevents the separation of any site from the rest bulk unless all the effective hopping parameters are zero. As a result, there will be only one transition. This is clearly seen in comparing Z_1 and Z_3 in Fig. 3(d).

The quasiparticle weight as a function of U/D is shown in Fig. 3(b). It is again seen that U_c/D is comparable for all three cases. As in the one-orbital case, this illustrates that the reduction of U_c for the modulated lattices originates from the band-narrowing effect.

Implications for $(K,Tl)_yFe_xSe_2$. Our results imply that the critical interaction strength for the Mott transition will be smaller in $(K,Tl)_yFe_xSe_2$ than in iron arsenides and 11 iron chalcogenides. This provides the basis for a Mott-insulating state in the parent $(K,Tl)_yFe_xSe_2$, even when one assumes the same strength of Coulomb interaction across all families of iron-based superconductors.

The Mott-insulating nature of the parent $(K,Tl)_yFe_xSe_2$ is supported by experiments. As already mentioned, the materials for both $x = 1.5$ and $x = 1.64$ have a large electrical resistivity with an insulating temperature dependence [12, 19]. Furthermore, the insulating behavior in the electrical resistivity is already observed in the paramagnetic phase. Relatedly, the optical conductivity is not only strongly suppressed below about 0.7 eV, but also small in magnitude. For reference, the value of the optical conductivity is comparable to that of the insulating $YBa_2Cu_3O_{6+x}$ with a slight off-stoichiometry $x = 0.2$ [33]. Finally, magnetic order is known to exist in $TlFe_xSe_2$ at x close to 1.5 [34]. Taken together, these experiments suggest that the insulating state is of the Mott type.

We note that in compounds with Fe content close to $x = 1.6$, the ordered vacancies have a different pattern [12, 18]. However, because we have shown that the Mott localization is a result of vacancy-ordering induced band narrowing, our argument will also apply to these systems. Band narrowing is

expected on the ground of general considerations given here, and can also be seen in the LDA results [22].

To summarize, we have used a two-orbital model in 1/4-depleted lattices to demonstrate that ordered vacancies enhance the tendency for Mott transition, and that this enhancement originates from a vacancy-induced kinetic-energy reduction. Our qualitative conclusion is expected to apply to the more realistic five-orbital model. Based on our calculations, we propose that the insulating parent of the $(K,Tl)_yFe_xSe_2$ superconductors is a Mott insulator at ambient pressure.

We thank J. Dai, M. Fang, and T. Xiang for useful discussions. This work was supported by NSF Grant No. DMR-1006985 and the Robert A. Welch Foundation Grant No. C-1411 (R.Y. and Q.S.), and U.S. DOE at LANL under Contract No. DE-AC52-06NA25396 (J.-X.Z.).

-
- [1] Y. Kamihara *et al.*, *J. Am. Chem. Soc.*, **130**, 3296 (2008).
 - [2] Z. A. Ren *et al.*, *Chin. Phys. Lett.*, **25**, 2215 (2008).
 - [3] C. de la Cruz *et al.*, *Nature* **453**, 899 (2008).
 - [4] M. M. Qazilbash *et al.*, *Nat. Phys.* **5**, 647 (2009).
 - [5] W. Z. Hu *et al.*, *Phys. Rev. Lett.* **101**, 257005 (2008).
 - [6] A. V. Boris *et al.*, *Phys. Rev. Lett.* **102**, 027001 (2009).
 - [7] J. Yang *et al.*, *Phys. Rev. Lett.* **102**, 187003 (2009).
 - [8] Q. Si and E. Abrahams, *Phys. Rev. Lett.* **101**, 076401 (2008).
 - [9] Q. Si, E. Abrahams, J. Dai, and J.-X. Zhu, *New J. Phys.* **11**, 045001 (2009); Q. Si, *Nat. Phys.* **5**, 629 (2009).
 - [10] A. Kutepov *et al.*, *Phys. Rev. B* **82**, 045105 (2010).
 - [11] J. Guo *et al.*, *Phys. Rev. B* **82**, 180520 (2010).
 - [12] M. Fang *et al.*, arXiv:1012.5236.
 - [13] Y. Zhang *et al.*, arXiv:1012.5980.
 - [14] T. Qian *et al.*, arXiv:1012.6017.
 - [15] D. Mou *et al.*, arXiv:1101.4556.
 - [16] I. R. Shein and A. L. Ivanovskii, arXiv:1012.5164.
 - [17] Z. Wang *et al.*, arXiv:1101.2059.
 - [18] W. Bao *et al.*, arXiv:1102.0830.
 - [19] D. M. Wang *et al.*, arXiv:1101.0789.
 - [20] Z. G. Chen *et al.*, arXiv:1101.0572.
 - [21] J.-X. Zhu *et al.*, *Phys. Rev. Lett.* **104**, 216405 (2010).
 - [22] C. Cao and J. Dai, arXiv:1101.0533.
 - [23] X-W Yan *et al.*, arXiv:1012.5536.
 - [24] C. Cao and J. Dai, arXiv:1012.5621.
 - [25] I. A. Nekrasov and M. V. Sadovskii, arXiv:1101.0051.
 - [26] L. Zhang and D. J. Singh, *Phys. Rev. B* **79**, 094528 (2009).
 - [27] S. Raghu *et al.*, *Phys. Rev. B* **77**, 220503(R) (2008).
 - [28] S. Graser *et al.*, *New J. of Phys.* **11**, 025016 (2009).
 - [29] L. de' Medici *et al.*, *Phys. Rev. B* **72**, 205124 (2005).
 - [30] R. Yu and Q. Si, arXiv:1006.2337.
 - [31] S. Florens and A. Georges, *Phys. Rev. B* **70**, 035114 (2004).
 - [32] E. Zhao and A. Paramekanti, *Phys. Rev. B* **76**, 195101 (2007).
 - [33] J. Orenstein *et al.*, *Phys. Rev. B* **42**, 6342 (1990).
 - [34] L. Häggström *et al.*, *J. Magn. Magn. Mater.* **98**, 37 (1991).